International Journal of Nanomedicine

Dovepress
open access to scientific and medical research

Open Access Full Text Article

ORIGINAL RESEARCH

Salvianolic acid B protects against myocardial damage caused by nanocarrier TiO_2; and synergistic anti-breast carcinoma effect with curcumin via codelivery system of folic acid-targeted and polyethylene glycol-modified TiO_2 nanoparticles

This article was published in the following Dove Press journal:
International Journal of Nanomedicine
2 November 2016
Number of times this article has been viewed

Lingling Ding[1–3]
Jiawei Li[1,2]
Rui Huang[1,2]
Zhidong Liu[1,2]
Chunhua Li[1–3]
Shaozi Yao[1,2]
Jinyan Wang[1,2]
Dongli Qi[1,2]
Nan Li[1,2]
Jiaxin Pi[1,2]

[1]Tianjin State Key Laboratory of Modern Chinese Medicine, Institute of Traditional Chinese Medicine, Tianjin University of Traditional Chinese Medicine, [2]Engineering Research Center of Modern Chinese Medicine Discovery and Preparation Technique, Tianjin University of Traditional Chinese Medicine, [3]Tianjin International Joint Academy of Biomedicine, Tianjin, People's Republic of China

Correspondence: Zhidong Liu; Jiawei Li
Tianjin State Key Laboratory of Modern Chinese Medicine, Institute of Traditional Chinese Medicine, Tianjin University of Traditional Chinese Medicine, 88 Yuquan Road, Nankai, Tianjin 300193, People's Republic of China
Tel +86 22 5959 6153
Email lonerliuzd@163.com; lijiawei1981@163.com

Abstract: Targeted delivery by the folate ligand is an effective way to enhance an anti-breast carcinoma effect, due to its high affinity for the folate receptor, which is overexpressed in many tumor cells. In this study, we firstly synthesized a folic acid (FA)-targeted and polyethylene glycol (PEG)-modified TiO_2 nanocarrier. Then, an FA-PEG-TiO_2 nanoparticle (NP) codelivery system loaded with curcumin and salvianolic acid B were prepared by emulsion evaporation–solidification at low temperature. The obtained folate-targeted NPs (FA-NPs) showed more cytotoxicity on MCF7 cells and MDA-MB-231 cells than a nontargeted NP group. Apart from a synergistic anti-breast cancer effect with curcumin, salvianolic acid B protects the cardiovascular system from oxidative injury by the TiO_2 nanocarrier. With coumarin 6 as a fluorescent probe to observe cellular uptake of NPs, the results of in vitro cellular uptake demonstrated FA-NPs exhibited higher cellular uptake and accumulation in MCF7 cells and MDA-MB-231 cells than nontargeted NPs. Then, in vivo biodistribution of NPs was further qualitatively and quantitatively confirmed by in vivo imaging. More importantly, the animal study further suggested that FA-NPs had significantly stronger antitumor effects via receptor-mediated targeted delivery. Consequently, FA-PEG-TiO_2 NPs loaded with curcumin and salvianolic acid B could be a promising drug-delivery system to treat breast cancer.

Keywords: breast cancer, codelivery, curcumin, FA-PEG-TiO_2, nanoparticles, salvianolic acid B

Introduction

Recently, breast cancer has been the leading cause of cancer-related deaths in women.[1] With respect to the treatment of breast tumors, chemotherapy plays a significant role despite some shortcomings, such as development of drug resistance, high toxicity, and limited regime of clinical usage.[2] In order to enhance anticancer effects and reduce these disadvantages as soon as possible, it is essential to develop a targeted codelivery antitumor drug-delivery system. With the development of nanotechnology, nanodrug-delivery systems have emerged as a promising strategy to accomplish this requirement, and can be delivered and accumulated at their targeted sites by either passive or active targeting mechanisms.[3] Additionally, synergy therapy, the simultaneous use of two or more drugs as a "one–two punch", has generated much interest, due to its effectiveness in cancer treatments.[4] Therefore, designing novel nanocarriers is beneficial toward achieving preferable antitumor effects.

submit your manuscript | www.dovepress.com
Dovepress
http://dx.doi.org/10.2147/IJN.S107767

As inorganic carrier material, TiO_2 nanoparticles (NPs) have attracted more attention in drug delivery and cancer therapy recently, due to their unique physical and chemical properties, eg, ultrasmall size, increased surface area per unit mass, chemical composition, surface structure, shape, aggregation, high stability, and low cost.[5] In particular, due to the fact that TiO_2 can generate highly reactive radical oxygen species under ultraviolet (UV)-light irradiation and lead to cancer-cell death, it is promising for a new class of photodynamic therapy agent.[6] For instance, Yin et al[4] compounded upconverting NPs with a mesoporous TiO_2 shell for near-infrared (IR)-triggered drug delivery and synergistic targeted cancer therapy. Their study demonstrated that it not only promised a targeted ability toward CD44-overexpressed cancer cells but also conferred controlled drug release by specific enzymes present in the tumor microenvironment. Despite promising effects in killing cancer cells, such treatments would be tough to conduct in clinical applications for the following reasons. Firstly, the reactive radical oxygen species generated by TiO_2 NPs are more likely to result in oxidative damage to normal tissues, especially the cardiovascular system.[7] Then, UV light cannot penetrate deeply into human tissues, thus limiting its application on superficial tumors.[8] Additionally, UV-mediated reactive oxygen species from TiO_2 NPs have a very short life span, so they would not be able to produce a persistent cancer-killing effect.[9] To overcome these challenges, some researchers have designed TiO_2 NPs modified with –OH, $–NH_2$, or –COOH surface groups.[10] In our study, TiO_2 NPs were modified with an amino group, polyethylene glycol $(PEG)_{2000}$, and folate ligand, which not only had an anti-breast cancer effect but could also prolong circulation time and deliver drugs to tumor sites via the targeted group. More importantly, in our study, salvianolic acid B (Sal B) was used to protect the cardiovascular system from oxidant damage by the TiO_2 nanocarrier; meanwhile, Sal B also played a part in the anti-breast cancer effect.

Sal B is a major water-soluble polyphenolic acid extracted from Lamiaceae radix *Salvia miltiorrhiza*, which is a common herbal medicine that has been clinically used in China for thousands of years as a blood circulation-accelerating agent and antioxidant.[11] Apart from anti-inflammation, anticoagulation, and antioxidation, Sal B has also shown obvious anticancer activity in a variety of cancer cell lines, including prostate, breast, liver, and head and neck squamous cell cancers.[12–14] Curcumin (Cur) is diferuloylmethane or 1,7-bis(4-hydroxy-3-methoxyphenyl)-1,6-hepadiene-3,5-dione, and has presented a comprehensive array of pharmacological properties, such as anti-inflammatory, antioxidant, anticancer, antimicrobial, antiparasitic, antitumor, antiangiogenic, and antimutagenic effects.[15] Currently, Cur is used mainly for inhibiting cancer in a variety of cell lines, and has expressed obvious antitumor effects, eg, in breast cancer and ovarian cancer.[16,17] Therefore, we chose Cur and Sal B as synergistic antitumor drugs, while Sal B also played a role in protecting myocardial damage caused by TiO_2 NPs.

Additionally, in order to prolong circulation time, surface modification of nanocarriers with PEG has emerged as a strategy to dramatically decrease the rapid mononuclear phagocyte-system uptake of NPs and to increase the blood-circulation half-life of the drugs, due to the enhanced permeability-and-retention effect in tumor tissues.[18] To address the targeting of NPs, there is an increasing requirement to enhance the efficient delivery of drugs to the targeted tumor site to obtain the potency of therapeutic agents via modifying nanocarriers with a target ligand. Compared with normal cells, cancer cells often excessively express several normal proteins on the cell surface, and these particular overexpressed proteins on cancer cells can be regarded as exceptional targets for active targeting.[19] The folate receptor, which is highly expressed on the cell membrane, especially in such malignancies in ovaries, brain, kidney, breast, myeloid cells, and lungs, is a useful targeting site for tumor-specific drug delivery, due to its low immunogenicity, ease of modification, and low cost.[20–22] Therefore, it is extremely advantageous to synthesize a better biomaterial: a folic acid (FA)-targeted and PEG-modified TiO_2 nanocarrier.

The goal of the current study was to obtain an FA-targeted and PEG modified TiO_2 NP-codelivery system loaded with Cur and Sal B to enhance the antitumor effect. When FA-PEG-TiO_2 NPs loaded with Cur and Sal B are administered via intravenous injection, the reactive radical oxygen species generated by TiO_2 NPs are more likely to result in oxidative damage to the cardiovascular system.[7] In order to cope with this challenge, not only does Sal B protect the cardiovascular system by its stronger antioxidant activity but also it can play an important role in the synergistic antitumor effect with Cur. Therefore, we compounded novel FA-PEG-TiO_2 nanocarriers for codelivery of Cur and Sal B to investigate the synergistic anti-breast carcinoma efficacy.

Materials and methods

Materials

NH_2-PEG_{2000}-COOH was purchased from Seebio Biotech Inc (Shanghai, China). FA, *N*-(3-dimethylaminopropyl)-*N*-ethylcarbodiimide (EDC), dicyclohexylcarbodiimide (DCC), *N*-hydroxysuccinimide (NHS), and 3-aminopropyltriethoxysilane (KH 550) were provided by Civi Chemical

Technology Co Ltd (Shanghai, China). TiO_2 NPs were purchased from Aladdin (Shanghai, China). Coumarin 6 was purchased from Thermo Fisher Scientific (Waltham, MA, USA). 1,10-Dioctadecyl-3,3,3,3-tetramethyl indotricarbocyanine iodide (DiR), near-IR lipophilic carbocyanine dye, was obtained from Biotium Inc (Hayward, CA, USA). Hoechst 33342 was provided by Thermo Fisher Scientific. Cell Counting Kit 8 (CCK-8) was purchased from Dojindo Laboratories (Kumamoto, Japan). Cur (purity ≥95%) was obtained from Saiyang Bio-technology Co Ltd (Xi'an, China). Sal B (purity ≥98%) was purchased from Zhongxin Pharmaceutical Group Co Ltd (Tianjin, China). Paraformaldehyde (4%) was obtained from Solarbio Science and Technology Co Ltd (Beijing, China). Caprylic/capric triglyceride (Miglyol 812), caprylocaproyl macrogolglycerides (Labrasol), lauroyl polyoxyl-32 glycerides (Gelucire 44/14) and Tween 80 were purchased from Fengli Jingqiu Commerce and Trade Co Ltd (Beijing, China). A glutathione (GSH) kit was obtained from Jiancheng Bioengineering Institute (Nanjing, China), and a bicinchoninic acid (BCA) kit was purchased from Solarbio Science and Technology.

Synthesis, purification, and characterization of FA-PEG-TiO_2

Synthesis of amino TiO_2

The amino TiO_2 was synthesized via two-step reactions.[23,24] Firstly, TiO_2 NPs (1 g, 5–10 nm) were dispersed in *n*-butyl alcohol in 10 mg/mL by ultrasonic dispersion (SB-3200D; Xinzi Biotechnology, Ningbo, China) to activate them. Then, the saline coupling agent KH550 was added to the TiO_2 NP solvent (v:v 1:9) along with some deionized water. The reaction was stirred for 2 hours in alkaline conditions at 85°C, and then desiccated 12 hours at 60°C after centrifugation (H1650-W; Xiangyi Centrifuge Instrument Co Ltd, Changsha, China). The collected product was stored at −20°C for the next use.

Synthesis of FA-PEG copolymer

The conjugation of FA to NH_2-PEG_{2000}-COOH was compounded based on a previously reported method, with minor modification.[3,21] Briefly, in order to form the activated FA, 600 mg of FA dissolved in 100 mL dehydrated dimethyl sulfoxide was reacted with DCC and NHS (FA:NHS:DCC molar ratio 1:5:5) under the protection of a nitrogen atmosphere away from light at ambient temperature for 18 hours. Then, the reaction solution was filtered through a 0.22 μm syringe filter (Millex-GP; EMD Millipore, Billerica, MA, USA) to remove undissolved dicyclohexylurea side product. In addition, NH_2-PEG_{2000}-COOH was added to the activated FA solution at a molar ratio of 10:1 (FA:PEG), which was stirred to react under the protection of the nitrogen atmosphere in the dark at room temperature for 8 hours. After precipitation with excess acetone, the sediment was dialyzed with a 3,500 Da molecular-weight-cutoff dialysis bag against Milli-Q water for 5 days. The precipitate was centrifuged, freeze-dried, and stored at −20°C for the next use.

Synthesis of FA-PEG-TiO_2 and PEG-TiO_2

FA-PEG-TiO_2 and PEG-TiO_2 were synthesized by forming an amido bond. To conjugate FA-PEG_{2000}-COOH or NH_2-PEG_{2000}-COOH with amino TiO_2, 600 mg of FA-PEG or 108 mg of NH_2-PEG_{2000}-COOH was dissolved in Dimethylsulfoxide (DMSO) along with 30 mg of EDC and 10 mg of NHS at ambient temperature. Then, this solution was added dropwise to 100 mg of amino TiO_2 aqueous solution. The reaction was allowed to proceed overnight away from light with slow stirring. For the purpose of removing unreacted compounds, a 3,500 Da molecular-weight-cutoff dialysis bag was applied to dialyze the reacting solution against Milli-Q water for 5 days. The reactant was centrifuged, freeze-dried, and stored at −20°C for the next use.

Characterization of amino TiO_2, FA-PEG, and FA-PEG-TiO_2

Fourier-transform infrared spectroscopy

In order to confirm further the structure of amino TiO_2, FA-PEG and FA-PEG-TiO_2 conjugate, Fourier-transform (FT)-IR spectroscopy (Spectrum 65; PerkinElmer, Waltham, MA, USA) was applied to evaluate. Five milligram of amino TiO_2, FA, NH_2-PEG_{2000}-COOH, FA-PEG, and FA-PEG-TiO_2 conjugate was mixed with 200 mg previously dried potassium bromide, and then the mixed powders were compressed to form a disk. Background scanning was conducted by using a pure potassium bromide disk before samples were analyzed. Spectra ranged from 400 to 4,000 cm^{-1}.

Differential scanning calorimetry of FA-PEG and FA-PEG-TiO_2

To verify further the structure of FA-PEG and FA-PEG-TiO_2, differential scanning calorimetry (DSC; Jade; PerkinElmer) was used to analyze them. To be specific, approximately 8 mg FA-PEG and FA-PEG-TiO_2 was added to the round sample cell and then compressed to a disk, after which a circular cover was added. The detection temperature was 0°C–400°C.

Proton nuclear magnetic resonance spectroscopy

The chemical structure of FA-PEG-TiO_2 conjugate was obtained using 600 MHz nuclear magnetic resonance (NMR)

spectroscopy (Bruker Optik GmbH, Ettlingen, Germany). FA-PEG-TiO_2 conjugate (5 mg) was dissolved in deuterated DMSO before analysis.

Elemental analysis

To confirm further the elemental composition of the synthetic nanocarrier FA-PEG-TiO_2, elemental analysis of FA-PEG-TiO_2 was conducted by transmission electron microscopy (TEM) energy-dispersive X-ray spectroscopy (Tecnai G2 F20; FEI, Hillsboro, OR, USA). The sample was prepared by adding the diluted samples to hydrophilic carbon-coated copper grids. Additionally, the carbon-coated copper grids were desiccated prior to analysis.

Preparation of FA-PEG-TiO_2 NPs loaded dually with curcumin and salvianolic acid B

Folate-targeted NPs were prepared according to a well-known emulsion evaporation–solidification method at low temperature. Briefly, according to the ratio of drug to carrier (1:1), 10 mg of FA-PEG-TiO_2 and 2 mg FA-PEG were dissolved in dichloromethane along with 8 mg Cur, which was regarded as the oil phase. Additionally, 4 mg Sal B was dispersed in ultrapure water, which was regarded as the aqueous phase. Then, quantities of glyceryl monostearate, Miglyol 812, and Gelucire 44/14 were added to play surfactant roles in the oil phase. Meanwhile, Tween 80 and Labrosol were obtained and regarded as surface-active agents in the aqueous phase. Then, the oil phase and oil surfactant were mixed after heating in a 70°C water bath. Likewise, the aqueous solution of Sal B was blended with the surfactant in the water phase under magnetic stirring. Ultimately, the aqueous phase was added dropwise into the oil phase under magnetic stirring in a 70°C water bath and the stirring continued, in order to volatilize the organic solvent. The obtained NP solution was placed in a 4°C freezer to solidify after filtering via 0.22 μm microfiltration. In addition, untargeted PEG-TiO_2 NPs loaded with Cur and Sal B were prepared according to the same method.

Characterization of nanoparticles

Firstly, particle size and ζ-potential of NPs and FA-NPs were determined by dynamic light scattering (Zetasizer Nano ZS; Malvern Instruments, Malvern, UK). The morphological examination of NPs was carried out via TEM (Tecnai G2 F20). Specifically, the sample was prepared by adding the diluted samples (desiccated prior to analysis) to hydrophilic carbon-coated copper grids. Additionally, in order to verify further whether NPs had formed or not, DSC was used for analysis. Approximately, 8 mg of Cur, Sal B, the physical mixture, blank NPs, and FA-NPs loaded with dual drugs were extracted to the round sample cell and then compressed to a disk, after which a circular cover was added. The detection temperature was 0°C–400°C.

In addition, to determine the encapsulation efficiency (EE) of FA-NPs, ultrahigh-speed centrifugation (Hitachi Koki, Tokyo, Japan) was used. Briefly, the NP samples were dissolved in alcohol and subsequently demulsified via ultrasound to obtain a total drug solution, which was centrifuged at 4,000 rpm for 30 minutes to obtain the supernatant. Then, the NP sample was diluted with ultrapure water, which was then centrifuged at 58,000 rpm for 1 hour to obtain the free drug. Finally, the supernatant was analyzed on an 1100 Ultra Performance Liquid Chromatography (UPLC) system (Waters Corporation, Milford, MA, USA) with detection wavelengths of 427 nm (Cur) and 288 nm (Sal B). EE was calculated thus:

$$EE = \frac{\text{Amount of drug in the nanoparticles}}{\text{Total drug in the nanoparticles}} \times 100\% \quad (1)$$

Cell culture and animals

Human breast cancer MCF7 cells were kindly provided by Shenyang Pharmaceutical University (Shenyang, China), the use was approved by the Animal Experimentation Ethics Committee of Tianjin International Joint Academy of Biotechnology. The cells were cultured in Dulbecco's Modified Eagle's Medium supplemented with 10% fetal bovine serum (HyClone; GE Healthcare, Little Chalfont, UK), 100 units/mL penicillin, and 100 mg/mL streptomycin, and maintained in an incubator at 37°C and 5% CO_2. Human breast carcinoma MDA-MB-231 cells were purchased from ATCC (Manassas, VA, USA) and were cultivated in L-15 medium (HyClone) added to 10% fetal bovine serum (HyClone), 100 units/mL penicillin, and 100 mg/mL streptomycin at 37°C in a humidified atmosphere containing 5% CO_2. Rat myocardial H9c2 cells were obtained from the Type Culture Collection of the Chinese Academy of Sciences (Shanghai, China). H9c2 cells were cultivated in Dulbecco's Modified Eagle's Medium supplemented with 10% fetal bovine serum (HyClone), 100 units/mL penicillin, and 100 mg/mL streptomycin and maintained in an incubator at 37°C and 5% CO_2. BALB/c nude mice (female, 6–7 weeks old, 20±2 g) were obtained from the Experimental Animal Center of Tianjin International Joint Academy of Biotechnology and raised at 25°C±1°C with access to food and water ad libitum in a specific pathogen-free environment. The protocol of animal experiments was approved by the Animal Experimentation Ethics Committee of Tianjin International Joint Academy of Biotechnology and followed the institutes guidelines for care of mice.

Cardioprotective effect of salvianolic acid B against TiO_2-induced injury in cardiac H9c2 cells

Cardiac H9c2 cells were seeded at a density of 10^4 cells/well into 96-well culture plates to evaluate cell viability. Then, H9c2 cells were cultured in six-well plates at 2×10^5 cells/well for measuring GSH. Briefly, H9c2 cells were firstly exposed to different concentrations of TiO_2 NP solution (0.02, 0.1, 0.5, 2.5, and 12.5 mM) to choose the proper concentration that induced oxidant damage on H9c2 cells. Then, H9c2 cells were incubated in the same concentration of TiO_2 NP solution to form an oxidant-damage model, meanwhile incubating in different concentrations of Sal B solution (5, 10, and 20 μM). After 24 hours, the CCK-8, BCA kit, and GSH kit were used to determine cell viability and GSH level.

Cytotoxicity assay

The cytotoxicity of FA-NPs on both MDA-MB-231 and MCF7 cells was evaluated using the CCK-8 assay. Specifically, MDA-MB-231 cells and MCF7 cells were seeded at a density of 10^4 cells/well in 96-well culture plates and cultured for 24 hours in order to adhere. Then, cells were incubated with blank-NPs, NPs, FA-NPs, and free Cur–Sal B solution (Sol) at appropriate Cur and Sal B concentrations (Cur 0.08, 0.4, 2.0, 10, and 50 μM; Sal B 0.01, 0.05, 0.25, 1.25, and 6.25 μM) for 24 or 48 hours. After incubation for 24 or 48 hours, 10 μL CCK-8 was added to each well and incubated for 2.5 hours (MDA-MB-231 cells) and 3 hours (MCF7 cells), respectively. After that, the plates were subjected to microplate reading (FlexStation 3; Molecular Devices LLC, Sunnyvale, CA, USA) for cell-viability assays at a wavelength of 450 nm. Cell viability was calculated thus:

$$\text{Cell viability } (\%) = \frac{A_s - A_b}{A_c - A_b} \times 100\% \qquad (2)$$

where A_s, A_c and A_b refer to the absorbance of the experimental wells, the control wells, and the blank wells, respectively (n=6).

Cellular uptake of FA-NPs and NPs in MCF7 and MDA-MB-231 cells

The cellular uptake experiment was performed by high-content screening analysis (PerkinElmer). Briefly, MCF7 and MDA-MB-231 cells were seeded at a density of 10^4 cells/well into 96-well culture plates and cultured for 24 hours. Then, the cells were exposed to coumarin 6-labeled NPs and FA-NPs at cytotoxicity-free concentrations, which were respectively incubated for 6, 12, 24, and 36 hours. After NP solutions had been removed and washed twice with phosphate-buffered saline, cells were solidified with 4% formaldehyde for 15 minutes and stained with Hoechst 33342 away from light for 30 minutes. Then, the 96-well plates were subjected to analysis in the high-content screening reader after being washed twice with phosphate-buffered saline.

In vivo biodistribution

In vivo biodistribution of FA-NPs was evaluated with an In Vivo Imaging System (IVIS) imaging system (PerkinElmer) in BALB/c-nude mice (female, 20±2 g) bearing MDA-MB-231 tumors. The tumor model was established via subcutaneous inoculation of MDA-MB-231 cells into the right armpit of BALB/c-nude mice at a density of 10^7. In order to effectively access the targeting of FA-NPs and drug accumulation in tumors and organs, DiR was used as a near-IR fluorescence probe, which was encapsulated in the NPs to form DiR-labeled NPs, in the same fashion as loading for Cur and Sal B. When the tumor volume ranged from 150 mm^3 to 200 mm^3, the nude mice, which had been divided randomly into two groups, were intravenously injected with DiR-labeled NPs and FA-NPs via the tail vein. Afterward, fluorescence distribution was visualized in the IVIS at predetermined times with an excitation wavelength of 710 nm and emission wavelength of 790 nm. Meanwhile, the nude mice were killed and autopsied (n=3), and tumors and other organs, including the heart, liver, spleen, lung, and kidney, were excised and imaged.

In vivo anti-tumor-growth study

In order to estimate further the tumor growth-inhibiting efficacy of the FA-NPs, the BALB/c-nude mice bearing MDA-MB-231 tumor model was established. Briefly, when tumor volume grew to approximately 50 mm^3, the nude mice were randomly divided into five groups (n=6), which were administrated with normal saline (NS), cisplatin (PT) injection, Sol, NPs, and FA-NPs (5 mg/kg Cur, 1.35 mg/kg Sal B, and 1 mg/kg PT) via intravenous injection into the tail vein once a day for 7 days. During the period of administration, the body weight of nude mice was measured daily by the use of an electronic balance, while a Vernier caliper was applied to survey the length and width of tumors daily. Tumor volume was calculated thus: $V = 0.5\ LW^2$, where length (L) is the longest diameter and width (W) the shortest diameter perpendicular to length. At 3 days after the last injection, the nude mice were killed via cervical dislocation, and tumor tissues and major organs were harvested and immersed in 10% formaldehyde solution for the purpose of histological examination.

Histological examination

For the sake of better observing microstructural changes in tumor tissues and hearts, histological analysis was performed by means of hematoxylin–eosin staining: tumor tissues and hearts were fixed in 10% formaldehyde solution, dehydrated for a while, embedded in paraffin, cut into 5 mm-thick sections, and then stained with hematoxylin–eosin. The histological section was observed with an optical microscope.

Statistical analysis

All numerical data are expressed as means ± standard deviation. In order to estimate the statistical significance, an unpaired two-tailed Student's *t*-test was applied to compare between two groups.

Results

Synthesis and characterization of FA-PEG-TiO_2

Scheme 1 illustrates the synthetic process of FA-PEG-TiO_2, which consisted of three synthetic procedures. Firstly, active TiO_2 NPs were transformed to amino TiO_2 by silane-coupling reaction (Scheme 1A). Then, the carboxylic moiety of FA was coupled to the amino group of NH_2-PEG_{2000}-COOH to form the conjugate of FA-PEG according to the previously reported method (Scheme 1B).[21] Ultimately, the terminal carboxyl close to PEG of FA-PEG was interacted with the amine group of amino TiO_2 under EDC and NHS, in order to obtain the nanocarrier of FA-PEG-TiO_2 (Scheme 1C).

Structure characterization for the intermediate products FA-PEG and amino TiO_2 was confirmed by FT-IR (Figure 1A and B). Spectra of amino TiO_2 had characteristic peaks at 3,435.67 cm^{-1}, 2,930.44 cm^{-1}, 1,117.6 cm^{-1}, 1,029.03 cm^{-1}, and 551.06 cm^{-1}. Among these, the broad peak at 3,435.67 cm^{-1} corresponded to the stretching vibration of O–H and N–H, which resulted from the superposition of the peaks of N–H and O–H. Additionally, 2,930 cm^{-1} stood for the stretching vibration of C–H in KH550. Meanwhile, 1,117.6 cm^{-1} and 1,029.03 cm^{-1} corresponded to the stretching vibration of Si–O–C in KH550, while, 551.06 cm^{-1} demonstrated the bending vibration of Ti–O–Ti. The characteristic peaks proved that KH550 was more likely to graft to the appearance of TiO_2 (Figure 1B).

Likewise, the FT-IR spectra of FA also showed characteristic peaks at 1,694.92 cm^{-1} and 1,606.06 cm^{-1} (Figure 1A),

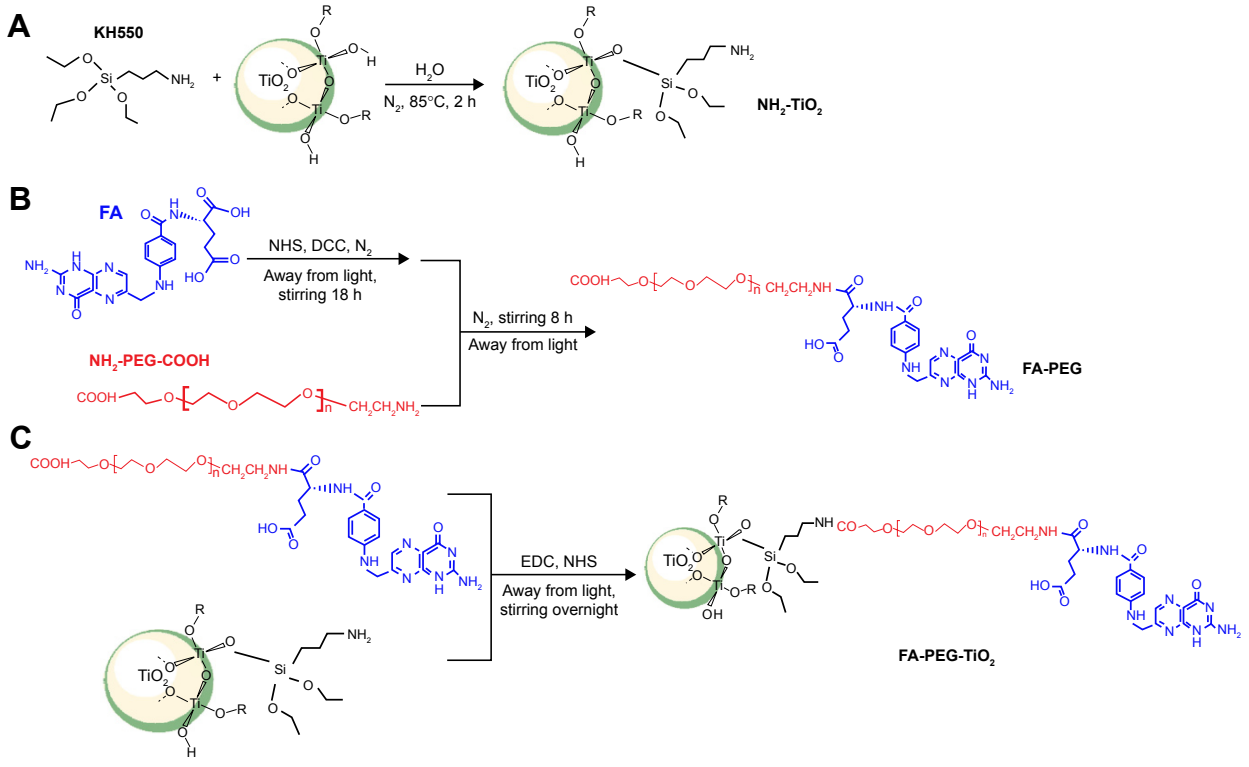

Scheme 1 Synthesis of the FA-PEG-TiO_2 nanocarrier.
Notes: (**A**) Synthesis of NH_2-TiO_2; (**B**) synthesis of FA-PEG; (**C**) synthesis of FA-PEG-TiO_2.
Abbreviations: EDC, N-(3-dimethylaminopropyl)-N-ethylcarbodiimide; NHS, N-hydroxysuccinimide; DCC, dicyclohexylcarbodiimide; FA, folic acid; PEG, polyethylene glycol; h, hours.

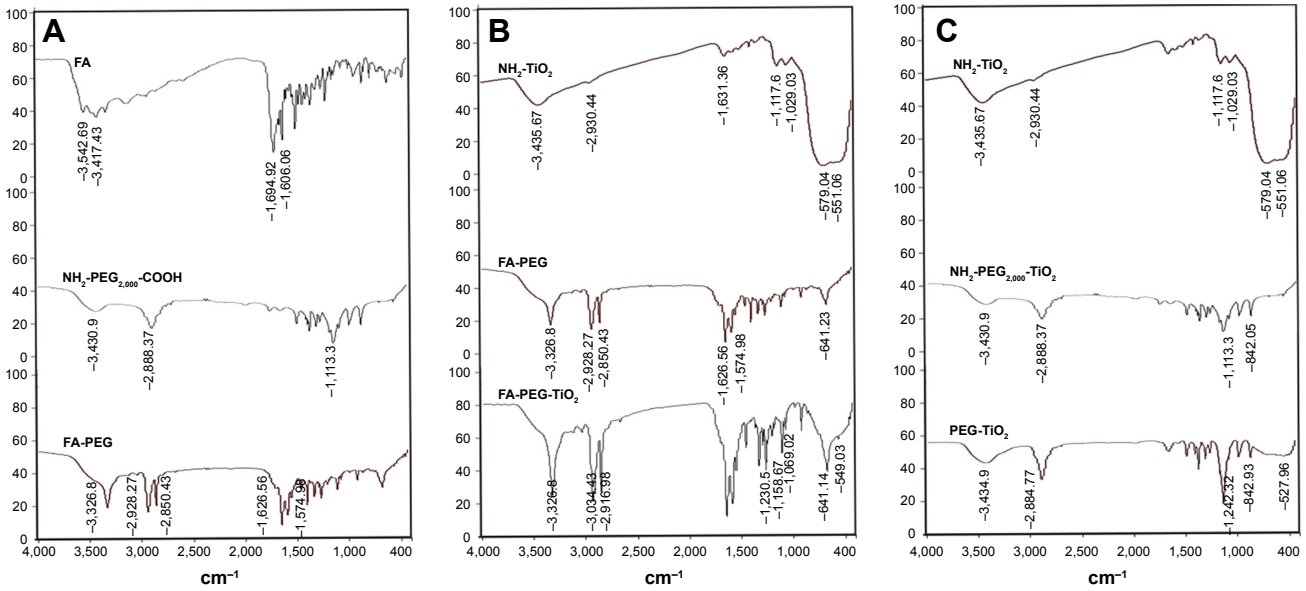

Figure 1 Fourier transform infrared (FT-IR) spectra of the FA-PEG-TiO_2 nanocarrier.
Notes: (**A**) FT-IR spectra of FA-PEG; (**B**) FT-IR spectra of FA-PEG-TiO_2; (**C**) FT-IR spectra of PEG-TiO_2.
Abbreviations: FA, folic acid; PEG, polyethylene glycol.

which were derived from the stretching vibration of the C=O bond of the carboxyl group and the C=C bond of the aromatic phenyl ring, respectively. The stretching of R–CH_2 of the alkyl group in the spectra of PEG was shown by a strong peak at 2,888.37 cm^{-1}, with the spectrum peak of 1,113.3 cm^{-1} for the stretching of the ether group of PEG. It was shown by the spectra of FA-PEG that dissociated peaks at 2,928.27 cm^{-1} and 2,850.43 cm^{-1} resulted from the alkyl group of PEG, along with strong peaks at 1,626.56 cm^{-1} and 1,574.98 cm^{-1} stemming from FA. Additionally, compared with the FT-IR spectra of FA-PEG, the characteristic peaks at 3,034.43 cm^{-1} and 2,916.98 cm^{-1} corresponded to the stretching vibration of C–H of the alkyl group in amino TiO_2, with the peaks of 1,069.02 cm^{-1}, 1,158.67 cm^{-1}, 1,230.5 cm^{-1} reflecting the stretching vibration of Si–O–C and Si–O–Si derived from amino TiO_2, as well as the weak peak of 549.03 cm^{-1} from the bending vibration of Ti–O–Ti (Figure 1B). Likewise, the structure of PEG-TiO_2 has also further been confirmed by FT-IR (Figure 1C), and was similar to the characteristics of FA-PEG-TiO_2 without the characteristic peaks of FA.

The DSC spectra in Figure 2A demonstrated that transformation peaks of FA-PEG-TiO_2 were approximately 300°C, appearing as two decalescence peaks at 225°C in DSC curve b in comparison to the DSC spectrum of FA-PEG. Also, the existence of Si and Ti in FA-NPs by elemental analysis is shown in Figure 2B. More importantly, the structure of FA-PEG-TiO_2 was further determined by hydrogen-nuclear magnetic resonance (^{1}H-NMR) (Figure 3). The peak at

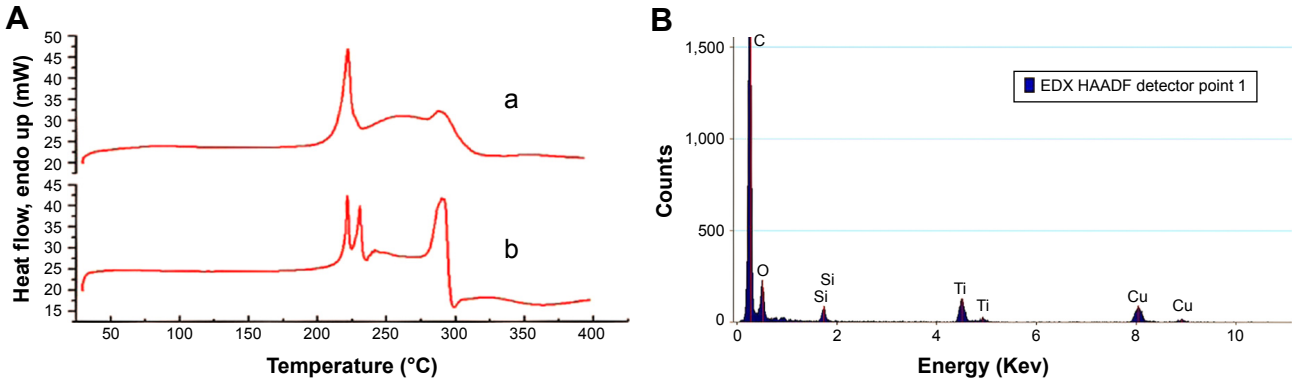

Figure 2 Characterization of differential scanning calorimetry (DSC) and element analysis of the FA-PEG-TiO_2 nanocarrier.
Notes: (**A**) DSC spectra of FA-PEG (a) and FA-PEG-TiO_2 (b); (**B**) element analysis of the FA-PEG-TiO_2 nanocarrier.
Abbreviations: FA, folic acid; PEG, polyethylene glycol; EDX, energy-dispersive x-ray spectroscopy; HAADF, high-angle annular dark field.

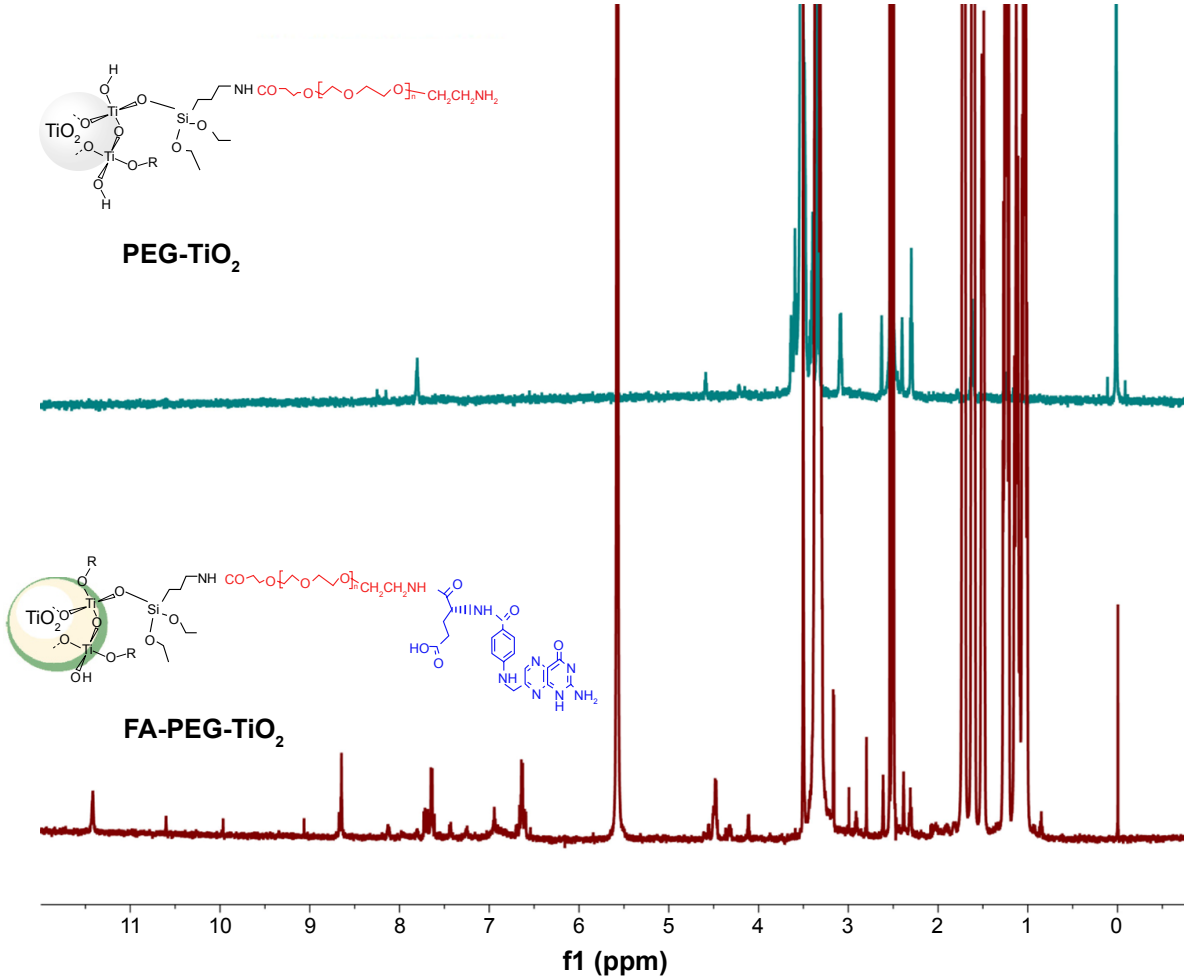

Figure 3 Proton nuclear magnetic resonance spectroscopy of PEG-TiO_2 and FA-PEG-TiO_2.
Abbreviations: FA, folic acid; PEG, polyethylene glycol.

7.65 ppm resulted from an aromatic proton of FA, 3.36 and 2.539 ppm deriving from the $–CH_2–CH_2–O$ bond of PEG and the NH–CO bond between TiO_2 and PEG, as well as 1–2 ppm resulting from the alkyl groups of FA and amino TiO_2. The ^{1}H-NMR of PEG-TiO_2 is shown in Figure 3, and was similar to FA-PEG-TiO_2 except for the characteristic peaks of FA. These structural characteristics verified the FA-PEG-TiO_2 nanocarrier had been synthesized successfully, and laid a foundation for the preparation of FA-PEG-TiO_2 NPs loaded with Cur and Sal B.

Preparation and characteristics of FA-PEG-TiO_2 nanoparticles loaded dually with curcumin and salvianolic acid B

Folate-targeted NPs were prepared according to a well-known emulsion evaporation–solidification technique at low temperature. Blank NPs and untargeted NPs were prepared by the same method. As shown in Table 1, the mean particle size of NPs was about 15–26 nm, particle-size distribution being shown in Figure 4A, and the polydispersity index was 0.2–0.5, demonstrating an acceptable particle-size distribution,

Table 1 Characterization of NPs and FA-NPs

	Particle size (nm)	Polydispersity index	ζ-potential (mV)	Curcumin (EE%)	Salvianolic acid B (EE%)
NPs	26.67±1.52	0.504±0.1	–7.79±1.54	48.6±0.42	44.1±2.43
FA-NPs	18.01±0.79	0.305±0.04	–7.80±2.01	52.2±0.06	44.3±0.35
Blank NPs	15.81±0.79	0.243±0.06	–1.98±1.01		

Note: Data presented as means ± standard deviation (n=3).
Abbreviations: NPs, nanoparticles; FA, folic acid; EE, encapsulation efficiency.

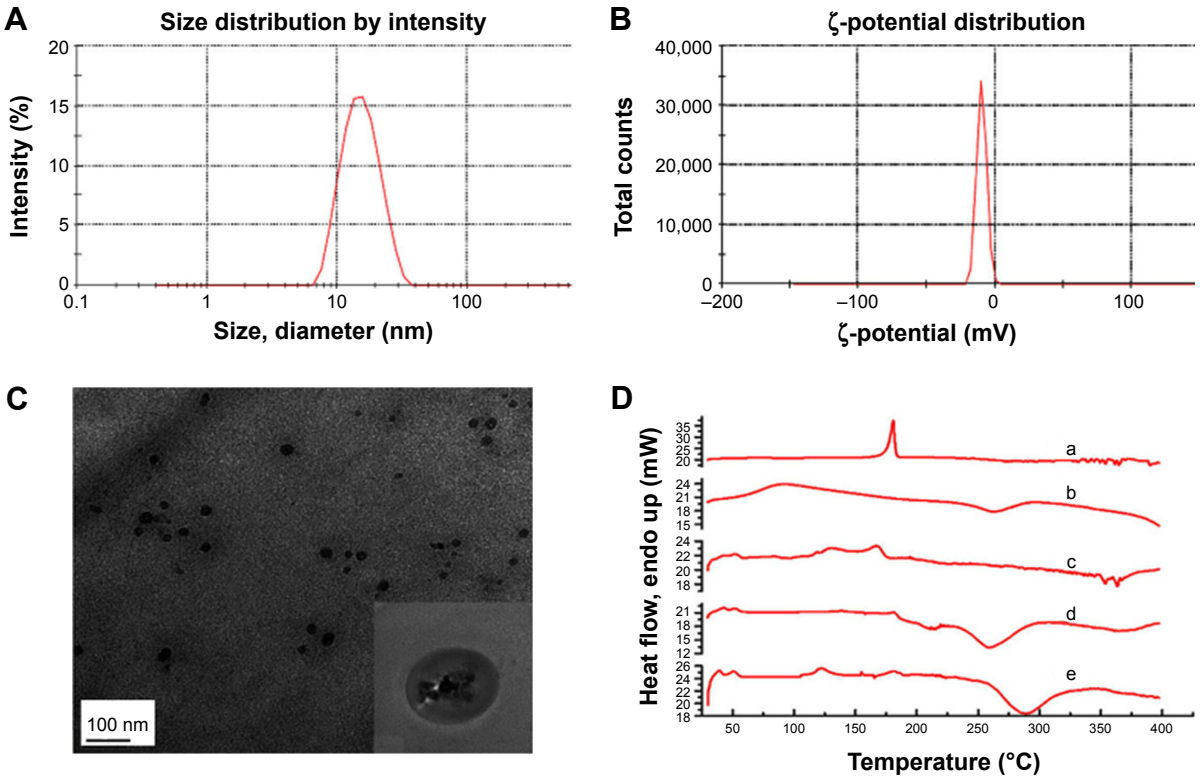

Figure 4 Characterization of FA-NPs.
Notes: (**A**) Particle size; (**B**) ζ-potential; (**C**) TEM; (**D**) DSC spectra (curcumin [a], salvianolic acid B [b], physical mixture [c], blank NPs [d], FA-NPs [e]).
Abbreviations: FA, folic acid; NPs, nanoparticles; TEM, transmission electron microscopy; DSC, differential scanning calorimetry.

while ζ-potential ranged from −1.98 to −7.79 mV (Figure 4B). FA-NPs and NPs indicated good loading capacities for Cur and Sal B, along with EEs of 48.3%–52.3% and 41.5%–46.3%, respectively, which suggested a similar ability to load drug for FA-NPs and NPs. The morphology of NPs was observed by TEM (Figure 4C), which showed rounded and well-distributed particles. The diameter of NPs detected by TEM was in accordance with dynamic light-scattering measurement, which was about 20 nm. NPs were characterized by DSC to confirm whether the drug was encapsulated in NPs. As observed in Figure 4D, the decalescence peaks of Cur at 170°C disappeared in DSC curve e and the decalescence peaks of Sal B were at about 75°C in DSC curve b, absent in the DSC curve e. Interestingly, there was a strong decalescence peak near 125°C, which was more likely to have occurred through the joint effects of interaction with the components in the NPs. As demonstrated by DSC spectra, Cur and Sal B were loaded into the NPs.

Cardioprotective effect of salvianolic acid B against TiO_2-induced injury in cardiac H9c2 cells

The ability of TiO_2 NPs in regulating cell viability in cardiac myoblast H9c2 cells was determined with the CCK-8 kit. As shown in Figure 5A, the cell viability of H9c2 cells significantly decreased with increased TiO_2 NP concentration (0.02, 0.1, 0.5, 2.5, and 12.5 mM; $P<0.05$). Among these concentrations of TiO_2 NPs, the cell viability of the 2.5 mM group and 12.5 mM group was 79.82% and 60.07%, respectively; therefore, the 2.5 mM TiO_2 NP group was chosen to form the oxidant-damage model in our study. As shown in Figure 5B, the cell viability of Sal B groups was higher than the TiO_2-only treatment group, and the GSH level of Sal B groups was lower than the TiO_2-only treatment group (Figure 5C), indicating that Sal B possessed a cardioprotective effect against TiO_2-induced injury in cardiac H9c2 cells. The protective effect of 10 μM Sal B was the strongest among all Sal B-treatment groups rather than 20 μM Sal B, after exposure on 2.5 mM of TiO_2 NPs for 24 hours, which was consistent with a previous study.[25]

Cytotoxicity assays of Cur- and Sal B-loaded NPs

It has been reported that Cur has obvious anti-breast cancer effects, and Sal B also possesses certain anticancer properties. Therefore, in this research, we evaluated the impact on cell viability of dual-drug-loaded FA-NPs

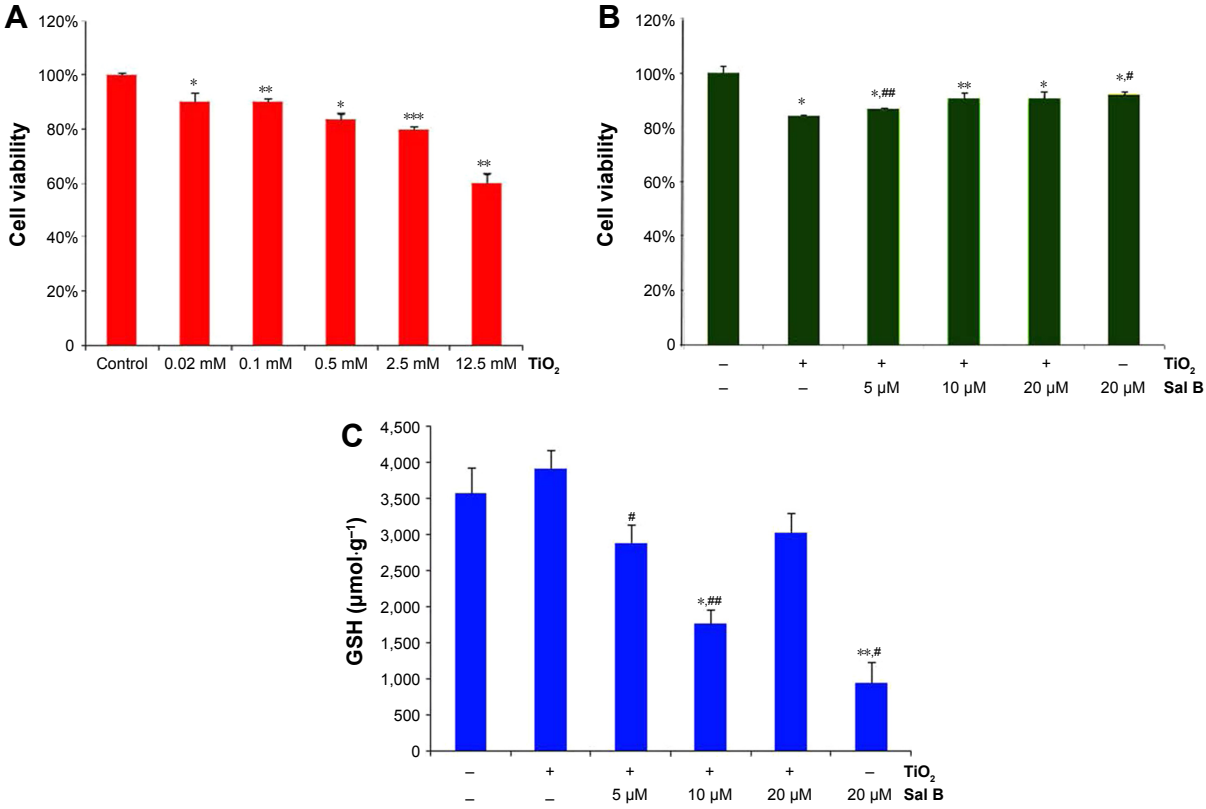

Figure 5 Cardioprotective effect of salvianolic acid B.

Notes: *$P<0.05$, **$P<0.01$, ***$P<0.001$ compared to control group; #$P<0.05$, ##$P<0.01$ compared to TiO_2 group. Data presented as means ± standard deviation (n=3). (**A**) Cell viability of H9c2 cells exposed to TiO_2 nanoparticles; (**B**) cell viability of H9c2 cells under the protection of salvianolic acid B; (**C**) GSH levels of H9c2 cells under the protection of salvianolic acid B.

Abbreviation: GSH, glutathione.

against the human breast cell lines of MCF7 and MDA-MB-231 compared with free Cur and Sal B solution or untargeted NPs at equivalent concentrations. As shown in Figure S1A, the cell viability of MCF7 cells exposed to blank NPs was more than 80% at doses of 0.08 μM, 0.4 μM, and 2 μM (according to the concentration of drug loaded into NPs) at 24 hours, whereas the survival rate was considerably below 80%, even less than 60% at a concentration of 10 μM and 50 μM, when MCF7 cancer cells were incubated after 48 hours in blank NPs. Likewise, as shown in Figure S1B, the cell viability of MDA-MB-231 cells gradually declined and almost exceeded 60%, in accordance with the increased doses at for both 24 h and 48 h incubation periods.

These verified blank NPs exerted more cytotoxic effects on MCF7 cells than on MDA-MB-231 cells when the concentration of blank NPs was over 2 μM. In addition, the cytotoxicity of MCF7 cells (Figure S1C and D) indicated that the survival rate of MCF7 cells gradually decreased with increasing drug dose when incubated for 24 and 48 hours. The cytotoxicity of 48 hours was more detrimental than 24 hours in MCF7 cells, except for the 6.25 μM Sal B and 50 μM Cur groups.

Likewise, the cytotoxicity of MDA-MB-231 cells was illustrated in Figure S1E and F, and was similar to the cytotoxicity results of MCF7 cells. Cytotoxicity statistics for MCF7 and MDA-MB-231 cells demonstrated that the detrimental effect exerted by FA-NPs was more than NPs and the cytotoxicity of FA-NPs was stronger than NPs alone on both MCF7 cells and MDA-MB-231 cells at the same time, which was associated with the folate receptor-mediated targeted function. The cytotoxicity of the Sol group was inferior to the NP group; however, NPs and FA-NPs had more harmful influence on MDA-MB-231 cells than on MCF7 cells.

Cellular uptake of nanoparticles

In order to observe the cellular uptake of FA-NPs and NPs, high-content analysis (PerkinElmer) was applied to investigate further coumarin 6-labeled NPs in MCF7 and MDA-MB-231 cells. Cellular uptake results demonstrated the fluorescence intensity of FA-NPs was obviously higher than NPs, and they were stronger than the Sol group in MCF7 cells (Figure 6A).

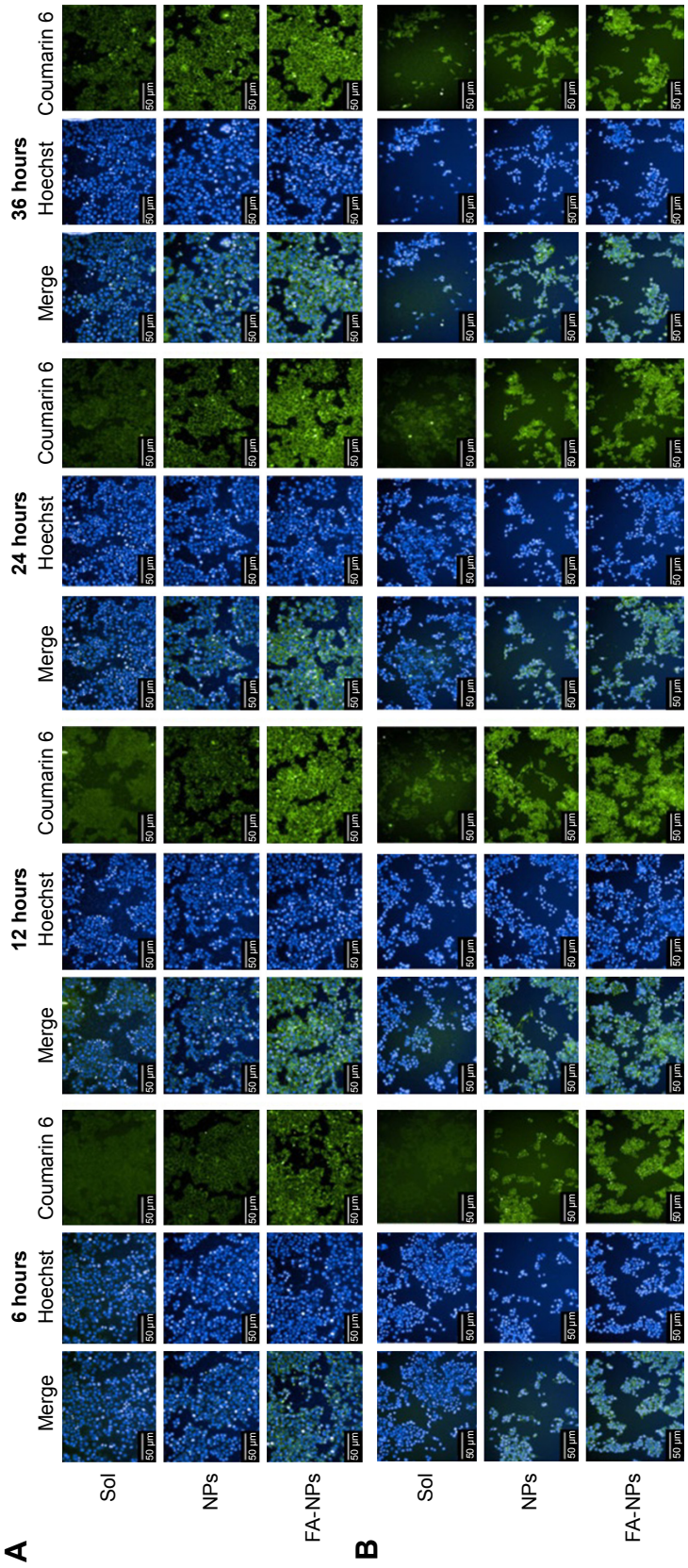

Figure 6 Cellular uptake of NPs at different time intervals.
Notes: (**A**) MCF7 cells; (**B**) MDA-MB-231 cells.
Abbreviations: Sol, free Cur-Sal B solution; NPs, nanoparticles; FA, folic acid; Cur, Curcumin; Sal B, Salvianolic acid B.

Their fluorescence intensity varied with time, with stronger fluorescence intensity at 12 and 24 hours and weaker fluorescence intensity at 6 and 36 hours. Cellular uptake of NPs in MDA-MB-231 cells is shown in Figure 6B. The fluorescence intensity of coumarin 6 was strongest at 12 hours compared to 6, 24, and 36 hours. Additionally, the fluorescence intensity of coumarin 6 in the FA-NP group was distinctly stronger than the NP and Sol groups and the fluorescence intensity of the NP group higher than the Sol group. The NPs distributed mainly in the cytoplasm of MCF7 and MDA-MB-231 cells, which was demonstrated by the green fluorescence of coumarin 6 in the cytoplasm and the blue fluorescence of Hoechst 33342 in cell nuclei.

In vivo biodistribution of nanoparticles

In this study, the IVIS (PerkinElmer) was used to evaluate the in vivo biodistribution and targeting of NPs by BALB/c-nude mice bearing MDA-MB-231 tumors. DiR was used as a fluorescent probe entrapped in the NPs, similarly to the loading of dual drugs. It was obvious that fluorescence could not be observed in untreated nude mice bearing breast cancer tumors (Figure 7A). The fluorescence of DiR in the FA-NP and NP groups gradually strengthened with time (Figure 7A), along with drug accumulation in tumor sites and other organs at 1, 2, 4, 6, 8, 12, 24, and 48 hours. The fluorescence of both NPs mainly concentrated on the liver tissues before 12 h, then focused on tumor issues and other organs. Finally, it was gradually eliminated from the body. BALB/c nude mice bearing breast carcinomata were killed to obtain tumors, hearts, livers, spleens, lungs, and kidneys, which were imaged with the IVIS (Figure 7B).

At 4 hours after tail-veil injection, the drug began to arrive at the tumor site with a weaker fluorescent signal; however, the liver was observed to have the strongest fluorescence intensity at 4 hours. Furthermore, fluorescence became strongest in tumor sites at 24 hours, and gradually decreased over time, similarly to previous research.[26] It was believed that the accumulation of FA-NPs was contributed to by angiogenic blood vessels and folate receptor-mediated targeting ability on the surface of tumor cells.[20] The fluorescence intensity of the FA-NP group was distinctly stronger than the NP group in tumor sites, at the same time point. For the sake of quantitative analysis, the fluorescence intensity of these organs mentioned is given in Figure 7C–F. These results demonstrated that fluorescent signals in tumor sites were highest at 24 hours and the fluorescence degree of the FA-NP group obviously stronger than the NP group at 4, 12, 24, and 36 hours. Compared with other organs, livers and lungs had the highest fluorescence intensity (Figure 7C–F), in particular livers, which was associated with an obvious entrapment of NPs by the reticuloendothelial system.[27]

In vivo antitumor study of nanoparticles

To estimate the in vivo tumor-growth inhibition of NPs, FA-NPs, NPs, PT, Sol, and NS were given to the female BALB/c-nude mice bearing MDA-MB-231 tumors, by intravenous injection via tail vein. During the injection, the body weight of mice was measured daily using an electronic balance, and a Vernier caliper was used to determine the length and width of tumors daily. As shown in Figure 8A, ability to inhibit tumor growth was as follows: FA-NPs > PT > NPs > Sol > NS, which was demonstrated by the growth curve of relative tumor volume. At 10 days, the relative tumor volume of the NP, Sol, PT, and NS groups was 2.39, 2.45, 2.31, and 2.76, respectively, in comparison to the 2.23 of the FA-NP group (Figure 8C). Additionally, Figure 8B illustrates that the body weight of mice decreased gradually with the prolongation of time, while compared with the PT, Sol, and NS groups, the body weight of the FA-NP and NP groups decreased more slowly. Significant differences in relative tumor volume and body weight of mice bearing MDA-MB-231 tumors are shown in Figure 8C and D.

Histological examination

Hematoxylin–eosin staining was applied to observe microstructural changes in tumor tissue and heart. Pathological sections of tumor tissues of the NS, NP, FA-NP, PT, and Sol groups showed pathological karyokinesis of the tumor cells (Figure 8E). Compared with the NS group, the FA-NP group had a spot of inflammatory cell infiltration and plenty of tumor-cell apoptosis that was more obvious than in the NP, PT, and Sol groups. Figure 8F demonstrates the histological change in heart tissues for all groups. Apart from the local inflammatory cell infiltration in the heart tissue of the PT group, other groups expressed normal heart morphological structure, especially the NP and FA-NP groups, which was consistent with our hypothesis.

Discussion

In antitumor-drug delivery, particle size plays an important role in determining antitumor effect. Particle diameter has to be appropriately controlled under 150 nm to meet the requirements of enhanced permeability-and-retention effect and decreased blood clearance.[27] In this work, FA-PEG-TiO_2 NPs had a particle size of 18.01±0.79–26.67±1.52 nm. Particle-size distribution was appropriate to deliver FA-PEG-TiO_2 NPs loaded with two drugs. Apart from particle size, ζ-potential is another important factor that can be used to

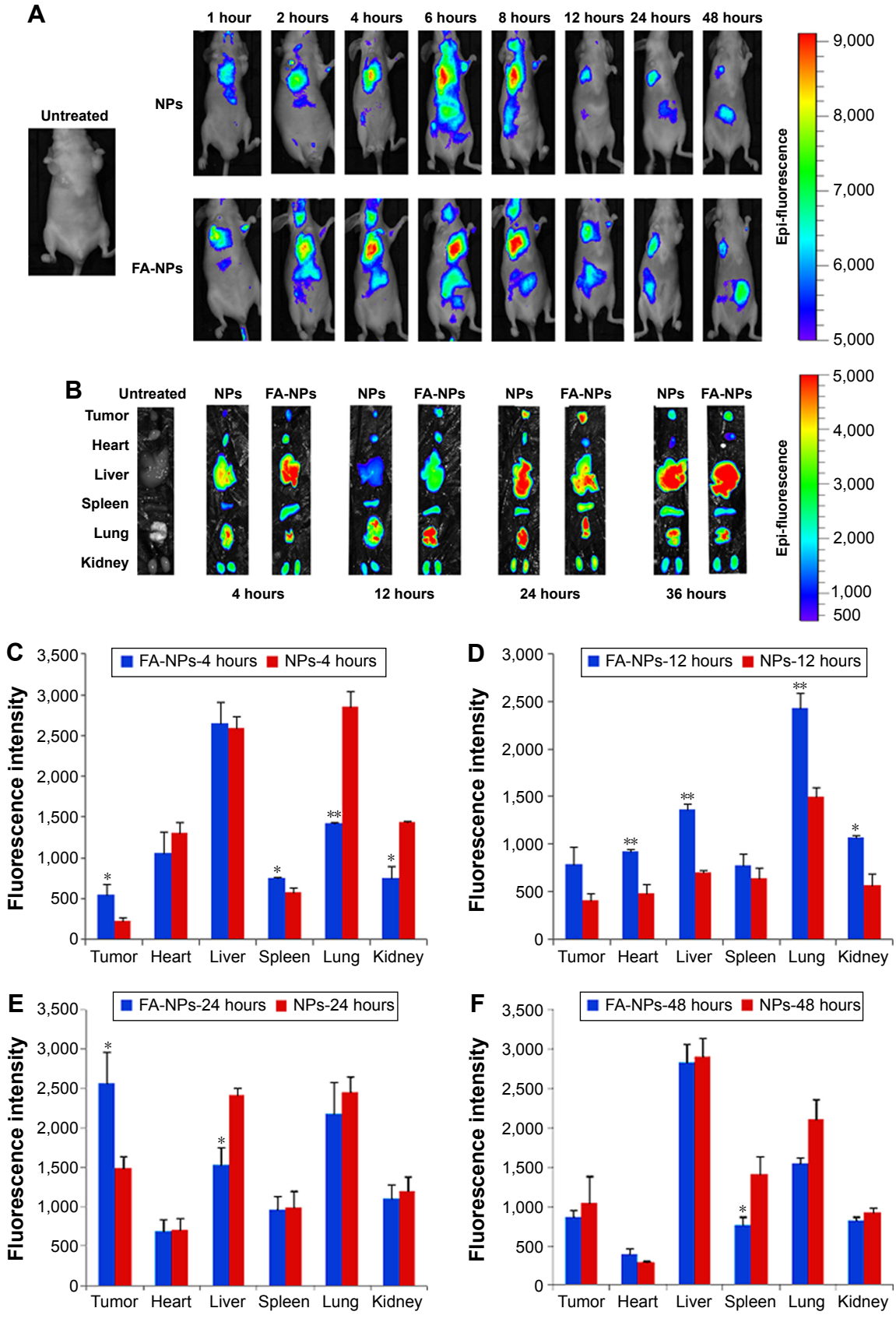

Figure 7 In vivo biodistribution of NPs.

Notes: *$P<0.05$, **$P<0.01$. Data presented as means ± standard deviation (n=3). (**A**) In vivo distribution of DiR-labeled NPs via tail-vein injection; (**B**) ex vivo fluorescence imaging of dissected organs at 4, 12, 24, and 48 hours postinjection. Fluorescence intensity of DiR-NPs and DiR-FA-NPs in different organs and tumors at 4 (**C**), 12 (**D**), 24 (**E**), and 48 (**F**) hours.

Abbreviations: DiR, 1,10-dioctadecyl-3,3,3,3-tetramethyl indotricarbocyanine iodide; NPs, nanoparticles; FA, folic acid.

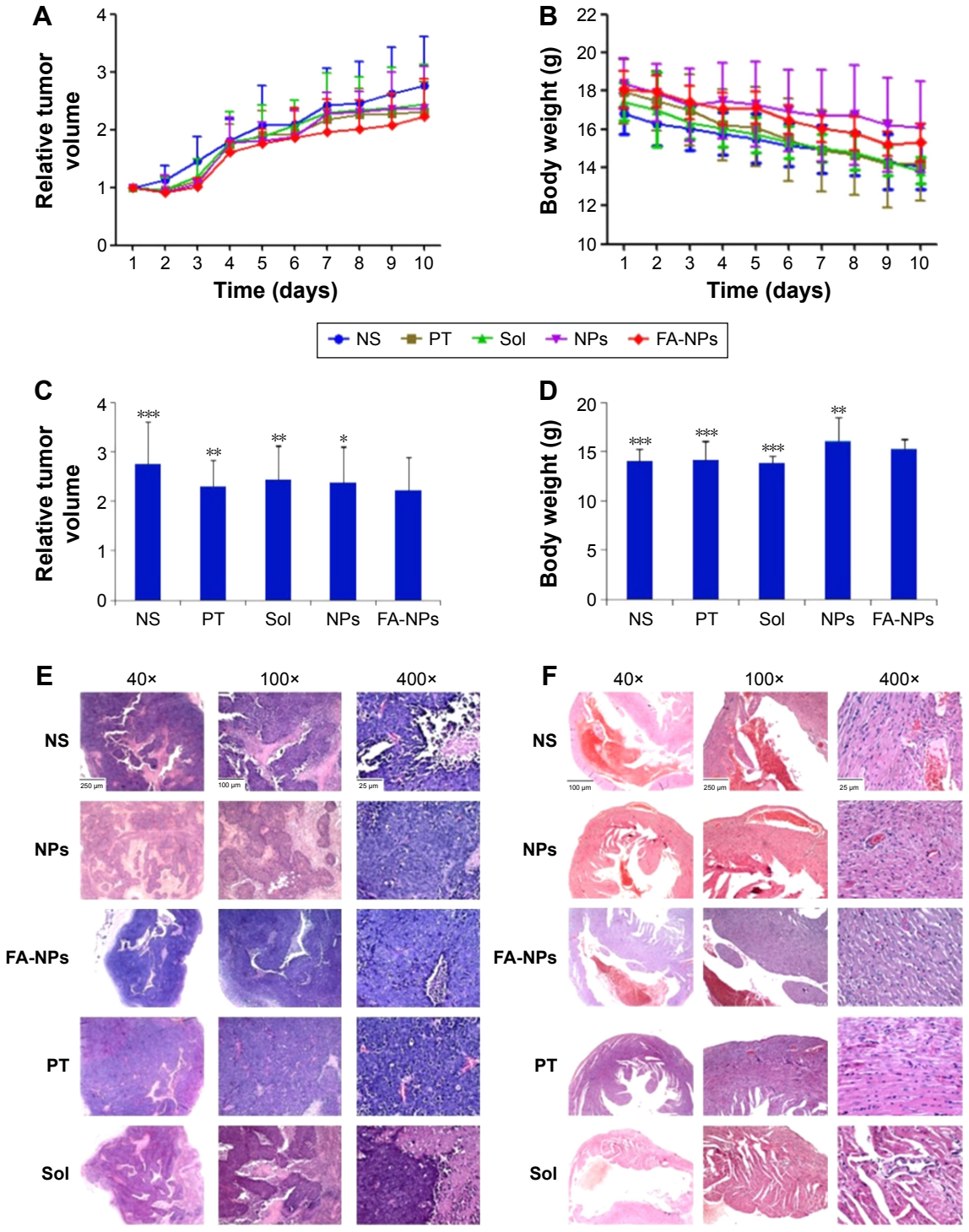

Figure 8 In vivo antitumor effects of different NPs on BALB/c nude mice bearing MDA-MB-231 tumors during the 10-day experimental period.
Notes: *$P<0.05$; **$P<0.01$; ***$P<0.001$. Data presented as means ± standard deviation (n=6). (**A**) Variation curves of relative tumor volume; (**B**) variation curves of body weight; (**C**) relative tumor volume at experimental end point (10th day); (**D**) body weight at experimental end point (10th day); (**E**) histologic sections of tumor; (**F**) histologic sections of heart.
Abbreviations: NS, normal saline; PT, cisplatin; Sol, free Cur–Sal B solution; NPs, nanoparticles; FA, folic acid; Cur, Curcumin; Sal B, Salvianolic acid B.

predict the fate of the NPs transited to the target site, as excess positive charge leads to opsonization with plasma proteins, resulting in interaction with cells of the reticuloendothelial system and deposition to the liver that destroys the targeted NP-delivery system.[28] After modification with FA and PEG, FA-PEG-TiO_2 NPs obtained a ζ-potential of −7.80±2.01 mV, which was extremely beneficial for the targeting of NPs and antitumor effect.

In addition, a folate receptor-mediated targeted NP-codelivery system demonstrates obvious anticancer activity,[19,21]

which not only improves selectivity for the tumor site but also reduces the side effects of therapeutic agents. Due to the fact that FA has high folate receptor-binding affinity index ($K_d = 1^{-10}$ M),[29] good tissue penetration, and rapid clearance from receptor-negative tissues,[22] we synthesized a FA-targeted and PEG-modified TiO_2 nanocarrier and prepared FA-PEG-TiO_2 NPs loaded with Cur and Sal B, in order to achieve synergistically targeted antitumor effects. After the modification of PEG_{2000}, FA-PEG-TiO_2 NPs had more chance of lessening the uptake of NPs by the rapid mononuclear phagocyte system and increasing the blood-circulation half-life of the drugs.[18]

Combination chemotherapy, eg, two or more drugs administered simultaneously or on the same day, exerts a higher and faster tumor-response rate than a single drug or sequential single-anticancer-drug combination for therapy for advanced and metastatic breast cancer.[30,31] In our work, apart from the anticancer effect of Cur and Sal B, the TiO_2 nanocarrier also exerted antitumor efficacy via generating reactive radical oxygen species in tumor sites.[4,5] It has been reported that Cur has stronger anticancer effects via multiple mechanisms. Firstly, Cur inhibits tumor-cell proliferation and induces the apoptosis of tumor cells by suppressing the Akt–mTOR–p70S6K pathway, activating the ERK1–2 signal pathway, and inducing the arrest of cell G_2/M.[32] Also, Cur is able to maintain body immunity during antitumor treatment, as it can supplement the NFκB activity of immune cells, due to the fact that oxidative stress induced by tumor cells interferes with the activation of NFκB inducing thymic atrophy and the death of T cells.[33,34] Moreover, Cur has been found to interfere with the PI3K–Akt signaling pathway, leading to suppression of cell proliferation, invasion, and migration in various cancer cells, including triple-negative breast cancer cells,[35] and Cur inhibits angiogenesis and negatively regulates the expression of angiogenesis related-genes, eg, inhibiting *VEGF*, *MMP9*, *ANG1*, *ANG2*.[36–39] However, with respect to the anticancer mechanism of Sal B, Wang et al found that Sal B induced apoptosis in human glioma U87 cells through p38-mediated Reactive Oxygen Species (ROS) generation.[40] It has been reported that Sal B restrained the expression of COX2 and PG to inhibit or delay the growth of cancer cells.[41] Therefore, Cur and Sal B were chosen to be used as anti-breast cancer drugs in our nanoconjugate. The in vivo antitumor results were exactly consistent with what we expected.

The protective effect on the cardiovascular system is demonstrated in Figure 4, which indicated that Sal B treatment can enhance cell viability. Compared with TiO_2 treatment alone, the number of viable cells gradually increased in Sal B-treatment groups with concentrations of 5, 10, and 20 μM (5 μM Sal B, $P<0.01$), although the 10 and 20 μM Sal B groups with similar cell viability (90.5% and 90.8%) were not statistically significantly different ($P>0.05$). GSH levels also showed a protective effect on the cardiovascular system, indicating the protective effect of 10 μM Sal B was the strongest among the three Sal B-treatment groups after exposure to 2.5 mM TiO_2 for 24 hours, consistent with a previous report.[25] It was more likely that the concentration of 20 μM Sal B was so high that it exerted a harmful effect on H9c2 cells, which can be demonstrated by the results of cellular viability of the 20 μM Sal B-only treatment group.

Cytotoxicity experiments demonstrated that FA-NPs and NPs showed concentration-dependent and time-dependent cytotoxicity, except for the 6.25 μM Sal B and 50 μM Cur groups at 24 and 48 hours. Perhaps it was the higher drug concentration that led to lower cell viability, which would cause more errors during the experiment. Meanwhile, the cytotoxicity of FA-NPs was stronger than NPs on both MCF7 cells and MDA-MB-231 cells at the same time, which was associated with folate receptor-mediated targeted function. In addition, results of cellular uptake of NPs manifesting fluorescence intensity of coumarin 6 in cells varied with time, showing time-dependent cellular uptake. Notably, the fluorescence intensity of the FA-NP group was distinctly stronger than the NP and Sol groups. On the whole, the cellular results suggested increased cytotoxicity and cellular uptake of FA-NPs, which would exhibit great superiority in antitumor drug delivery by significantly enhancing the intracellular accumulation of drugs to kill cancer cells more effectively.

In the study of in vivo biodistribution, DiR was used as a near-IR fluorescence probe loaded into the NPs. In vivo distribution of FA-NPs was observed by the IVIS at an excitation wavelength of 710 nm and emission wavelength of 790 nm, which suggested the fluorescence intensity of DiR in the FA-NP and NP groups gradually increased with the extension of time, along with the drug accumulation in tumor sites and other organs at a particular moment in time. Simultaneously, the fluorescence signal of the FA-NP group was distinctly stronger than NPs in tumor sites, reaching a maximum in 24 hours, similarly to a previous study.[26] It is believed that the accumulation of FA-NPs is contributed to angiogenic blood vessels and folate receptor-mediated targeting ability on the surface of tumor cells.[20]

Furthermore, study of the in vivo antitumor effect of NPs indicated the improved accumulation and penetration of FA-NPs at the tumor site, and achieved anticipated enhanced anti-tumor-growth efficacy in vivo. More importantly,

histopathology evaluation also verified these results. In spite of local inflammatory cell infiltration in the heart tissue of the PT group, other groups showed normal heart morphological structure, especially the NP and FA-NP groups, consistent with the expected result. It is more likely that the Sal B played a significant role in protecting against cardiovascular damage stemming from the TiO_2 NPs.[7,11]

Conclusion

In our study, an FA-PEG-TiO_2 nanocarrier was synthesized to load Cur and Sal B in order to obtain folate-targeted NPs to enhance an anti-breast cancer effect. The data showed that FA-NPs exhibited higher cytotoxicity, higher antiproliferative activity, and improved intracellular uptake on MCF7 and MDA-MB-231 cells. In vivo animal studies revealed better biodistribution and targeted ability in tumor sites, as well as improved antitumor efficacy of FA-NPs in comparison to untargeted NPs. To expand on our project, we will conduct long-term toxicity and pharmacokinetic experiments on the basis of this study in the near future. The improved anti-breast cancer effect demonstrated that the FA-PEG-TiO_2 NP-codelivery system would be a promising approach for the targeted therapy of breast cancer. Therefore, it can be concluded that the NP-based FA-PEG-TiO_2 developed is promising for the treatment of tumors.

Acknowledgments

We thank Dr Jiawei Li and Dr Zhidong Liu for their substantial contributions to concepts and design. Meanwhile, we appreciate Weibing Duan and Qian Zhang for their help on the animal experiments. We express our gratitude to Dr Xinggang Yang who offered us MCF7 cells from Shenyang Pharmaceutical University. This study was financially supported by the Program for The Research Plan of Application Foundation and Frontier Technology in Tianjin (Natural Science Funds) (16JCYBJC282000).

Disclosure

The authors report no conflicts of interest in this work.

References

1. Jemal A, Center MM, DeSantis C, Ward EM. Global patterns of cancer incidence and mortality rates and trends. *Cancer Epidemiol Biomarkers Prev*. 2010;19:1893–1907.
2. Sadzuka Y, Yamashita Y, Sonobe T. Effects of glutamate transporter inhibitors on the antitumor activity of doxorubicin. *Clin Cancer Res*. 2002; 8:3943–3947.
3. Wang L, Li M, Zhang N. Folate-targeted docetaxel-lipid-based-nanosuspensions for active-targeted cancer therapy. *Int J Nanomedicine*. 2012;7: 3281–3294.
4. Yin M, Ju E, Chen Z, Li Z, Ren J, Qu X. Upconverting nanoparticles with a mesoporous TiO_2 shell for near-infrared-triggered drug delivery and synergistic targeted cancer therapy. *Chemistry*. 2014;20:14012–14017.
5. Murugan K, Dinesh D, Kavithaa K, et al. Hydrothermal synthesis of titanium dioxide nanoparticles: mosquitocidal potential and anticancer activity on human breast cancer cells (MCF-7). *Parasitol Res*. 2016;115:1085–1096.
6. Rozhkova EA, Ulasov I, Lai B, Dimitrijevic NM, Lesniak MS, Rajh T. A high-performance nanobio photocatalyst for targeted brain cancer therapy. *Nano Lett*. 2009;9:3337–3342.
7. Sheng L, Wang X, Sang X, et al. Cardiac oxidative damage in mice following exposure to nanoparticulate titanium dioxide. *J Biomed Mater Res A*. 2013;101:3238–3246.
8. Cai R, Kubota Y, Shuin T, Sakai H, Hashimoto K, Fujishima A. Induction of cytotoxicity by photoexcited TiO_2 particles. *Cancer Res*. 1992;52:2346–2348.
9. Blake DM, Maness PC, Huang Z, Wolfrum EJ, Huang J, Jacoby WA. Application of the photocatalytic chemistry of titanium dioxide to disinfection and the killing of cancer cells. *Sep Purif Rev*. 1999;28:1–50.
10. Thevenot P, Cho J, Wavhal D, Timmons RB, Tang L. Surface chemistry influences cancer killing effect of TiO_2 nanoparticles. *Nanomedicine*. 2008;4:226–236.
11. He Q, Zhang J, Chen F, Guo L, Zhu Z, Shi J. An anti-ROS/hepatic fibrosis drug delivery system based on salvianolic acid B loaded mesoporous silica nanoparticles. *Biomaterials*. 2010;31:7785–7796.
12. Hao Y, Xie T, Korotcov A, et al. Salvianolic acid B inhibits growth of head and neck squamous cell carcinoma in vitro and in vivo via cyclooxygenase-2 and apoptotic pathways. *Int J Cancer*. 2009;124: 2200–2209.
13. Zhao Y, Hao Y, Ji H, et al. Combination effects of salvianolic acid B with low-dose celecoxib on inhibition of head and neck squamous cell carcinoma growth in vitro and in vivo. *Cancer Prev Res (Phila)*. 2010;3:787–796.
14. Zhao Y, Guo Y, Gu X. Salvianolic acid B, a potential chemopreventive agent, for head and neck squamous cell cancer. *J Oncol*. 2011; 2011:534548.
15. Cartiera MS, Ferreira EC, Caputo C, Egan ME, Caplan MJ, Saltzman WM. Partial correction of cystic fibrosis defects with PLGA nanoparticles encapsulating curcumin. *Mol Pharm*. 2009;7:86–93.
16. Aggarwal BB, Kumar A, Bharti AC. Anticancer potential of curcumin: preclinical and clinical studies. *Anticancer Res*. 2003;23:363–398.
17. Guo QT, Li X, Yang Y, et al. Enhanced 4T1 breast carcinoma anticancer activity by co-delivery of doxorubicin and curcumin with core-shell drug-carrier based on heparin modified poly (L-lactide) grafted polyethylenimine cationic nanoparticles. *J Biomed Nanotechnol*. 2014;10: 227–237.
18. Hua K, Din J, Cao Q, et al. Estrogen and progestin regulate HIF-1α expression in ovarian cancer cell lines via the activation of Akt signaling transduction pathway. *Oncol Rep*. 2009;21:893–898.
19. Balasubramanian S, Grija AR, Nagaoka Y, et al. Curcumin and 5-fluorouracil-loaded, folate-and transferrin-decorated polymeric magnetic nanoformulation: a synergistic cancer therapeutic approach, accelerated by magnetic hyperthermia. *Int J Nanomedicine*. 2014;9:437–459.
20. Low PS, Henne WA, Doorneweerd DD. Discovery and development of folic-acid-based receptor targeting for imaging and therapy of cancer and inflammatory diseases. *Acc Chem Res*. 2007;41:120–129.
21. Li TS, Yawata T, Honke K. Efficient siRNA delivery and tumor accumulation mediated by ionically cross-linked folic acid-poly (ethylene glycol)-chitosan oligosaccharide lactate nanoparticles: for the potential targeted ovarian cancer gene therapy. *Eur J Pharm Sci*. 2014;52:48–61.
22. Lu Y, Low PS. Folate-mediated delivery of macromolecular anticancer therapeutic agents. *Adv Drug Deliv Rev*. 2012;64:342–352.
23. Cheyne RW, Smith TA, Trembleau L, Mclaughlin AC. Synthesis and characterisation of biologically compatible TiO_2 nanoparticles. *Nanoscale Res Lett*. 2011;6:423.

24. Gonçalves RH, Schreiner WH, Leite ER. Synthesis of TiO_2 nanocrystals with a high affinity for amine organic compounds. *Langmuir*. 2010;26:11657–11662.
25. Wang M, Sun G, Sun X, et al. Cardioprotective effect of salvianolic acid B against arsenic trioxide-induced injury in cardiac H9c2 cells via the PI3K/Akt signal pathway. *Toxicol Lett*. 2013;216:100–107.
26. Feng Q, Yu MZ, Wang JC, et al. Synergistic inhibition of breast cancer by co-delivery of VEGF siRNA and paclitaxel via vapreotide-modified core-shell nanoparticles. *Biomaterials*. 2014;35:5028–5038.
27. Li SD, Huang L. Pharmacokinetics and biodistribution of nanoparticles. *Mol Pharm*. 2008;5:496–504.
28. Rekha MR, Sharma CP. Blood compatibility and in vitro transfection studies on cationically modified pullulan for liver cell targeted gene delivery. *Biomaterials*. 2009;30:6655–6664.
29. Antony AC. The biological chemistry of folate receptors. *Blood*. 1992;79:2807–2820.
30. Carrick S, Parker S, Thornton CE, Ghersi D, Simes J, Wilcken N. Single agent versus combination chemotherapy for metastatic breast cancer. *Cochrane Database Syst Rev*. 2009:CD003372.
31. Dear RF, McGeechan K, Jenkins MC, Barratt A, Tattersall MH, Wilcken N. Combination versus sequential single agent chemotherapy for metastatic breast cancer. *Cochrane Database Syst Rev*. 2013:CD008792.
32. Aoki H, Takada Y, Kondo S, Sawaya R, Aggarwal BB, Kondo Y. Evidence that curcumin suppresses the growth of malignant gliomas in vitro and in vivo through induction of autophagy: role of Akt and extracellular signal-regulated kinase signaling pathways. *Mol Pharmacol*. 2007;72:29–39.
33. Pal S, Bhattacharyya S, Choudhuri T, Datta GK, Das T, Sa G. Amelioration of immune cell number depletion and potentiation of depressed detoxification system of tumor-bearing mice by curcumin. *Cancer Detect Prev*. 2005;29:470–478.
34. Bhattacharyya S, Mandal D, Sen GS, et al. Tumor-induced oxidative stress perturbs nuclear factor-κB activity-augmenting tumor necrosis factor-α-mediated T-cell death: protection by curcumin. *Cancer Res*. 2007; 67:362–370.
35. Xu XB, Qin J, Liu WY. Curcumin inhibits the invasion of thyroid cancer cells via down-regulation of PI3K/Akt signaling pathway. *Gene*. 2014;546:226–232.
36. Hahm ER, Gho YS, Park S, Park C, Kim KW, Yang CH. Synthetic curcumin analogs inhibit activator protein-1 transcription and tumor-induced angiogenesis. *Biochem Biophys Res Commun*. 2004;321: 337–344.
37. Gururaj AE, Belakavadi M, Venkatesh DA, Marmé D, Salimath BP. Molecular mechanisms of anti-angiogenic effect of curcumin. *Biochem Biophys Res Commun*. 2002;297:934–942.
38. Bae MK, Kim SH, Jeong JW, et al. Curcumin inhibits hypoxia-induced angiogenesis via down-regulation of HIF-1. *Oncol Rep*. 2006; 15:1557–1562.
39. Matsuo M, Sakurai H, Koizumi K, Saiki I. Curcumin inhibits the formation of capillary-like tubes by rat lymphatic endothelial cells. *Cancer Lett*. 2007;251:288–295.
40. Wang ZS, Luo P, Dai SH, Liu ZB, Zheng XR, Chen T. Salvianolic acid B induces apoptosis in human glioma U87 cells through p38-mediated ROS generation. *Cell Mol Neurobiol*. 2013;33:921–928.
41. Cao W, Guo XW, Zheng HZ, Li DP, Jia GB, Wang J. Current progress of research on pharmacologic actions of salvianolic acid B. *Chin J Integr Med*. 2012;18:316–320.

Supplementary material

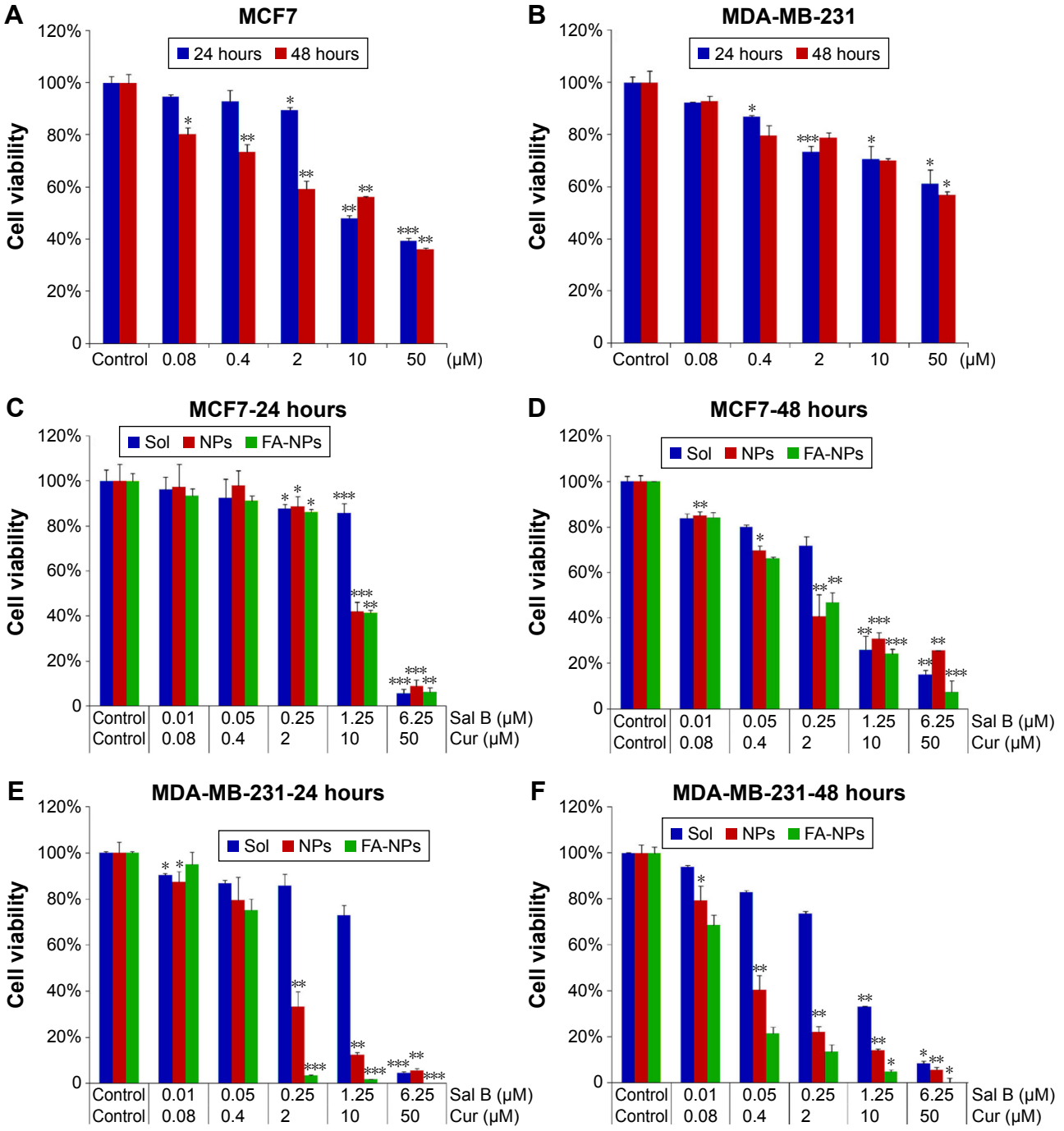

Figure S1 Cell viability of blank NPs, Sol, NPs, and FA-NPs on MCF7 cells and MDA-MB-231 cells.
Notes: *$P<0.05$; **$P<0.01$; ***$P<0.001$. Data presented as means ± standard deviation (n=3). (**A**) Cell viability of blank NPs on MCF7 cells; (**B**) cell viability of blank NPs on MDA-MB-231 cells; (**C**) cell viability of Sol, NPs, and FA-NPs incubating MCF7 cells for 24 hours; (**D**) cell viability of Sol, NPs, and FA-NPs incubating MCF7 cells for 48 hours; (**E**) cell viability of Sol, NPs, and FA-NPs incubating MDA-MB-231 cells for 24 hours; (**F**) cell viability of Sol, NPs, and FA-NPs incubating MDA-MB-231 cells for 48 hours.
Abbreviations: NPs, nanoparticles; Sol, solution (free Cur-Sal); FA, folic acid; Cur, curcumin; Sal, salvianolic acid.